PLOS ONE

RESEARCH ARTICLE

Simplified Models of Non-Invasive Fractional Flow Reserve Based on CT Images

Jun-Mei Zhang[1,2], Liang Zhong[1,2]*, Tong Luo[3], Aileen Mae Lomarda[1], Yunlong Huo[4], Jonathan Yap[1], Soo Teik Lim[1,2], Ru San Tan[1,2], Aaron Sung Lung Wong[1,2], Jack Wei Chieh Tan[1,2], Khung Keong Yeo[1,2], Jiang Ming Fam[1], Felix Yung Jih Keng[1,2], Min Wan[1,5], Boyang Su[1], Xiaodan Zhao[1], John Carson Allen[2], Ghassan S. Kassab[3], Terrance Siang Jin Chua[1,2], Swee Yaw Tan[1,2]

1 National Heart Center Singapore, 5 Hospital Drive, Singapore 169609, Singapore, **2** Duke-NUS Medical School, 8 College Rd, Singapore 169857, Singapore, **3** California Medical Innovations Institute, San Diego, CA 92121, United States of America, **4** Department of Mechanics and Engineering Science, College of Engineering, Peking University, Beijing, 100871, China, **5** School of Information Engineering, Nanchang University, Nanchang, Jiangxi, 330031, China

* zhong.liang@nhcs.com.sg

OPEN ACCESS

Citation: Zhang J-M, Zhong L, Luo T, Lomarda AM, Huo Y, Yap J, et al. (2016) Simplified Models of Non-Invasive Fractional Flow Reserve Based on CT Images. PLoS ONE 11(5): e0153070. doi:10.1371/journal.pone.0153070

Editor: Salvatore De Rosa, Magna Graecia University, ITALY

Received: October 12, 2015

Accepted: March 23, 2016

Published: May 17, 2016

Data Availability Statement: All relevant data are within the paper and its Supporting Information files.

Funding: This research is supported by the SingHealth Foundation Singapore under its Translational Research Grant (SHF/FG503P/2012), National Heart Center Singapore under its NHCS Centre Grant Seed Funding (NHCS-CGSF/2014/003), BMRC-NMRC Grant (BnB14Nov001), and Biomedical Research Council Research Grant (14/1/32/24/002).

Competing Interests: The authors have declared that no competing interests exist.

Abstract

Invasive fractional flow reserve (FFR) is the gold standard to assess the functional coronary stenosis. The non-invasive assessment of diameter stenosis (DS) using coronary computed tomography angiography (CTA) has high false positive rate in contrast to FFR. Combining CTA with computational fluid dynamics (CFD), recent studies have shown promising predictions of FFR_{CT} for superior assessment of lesion severity over CTA alone. The CFD models tend to be computationally expensive, however, and require several hours for completing analysis. Here, we introduce simplified models to predict noninvasive FFR at substantially less computational time. In this retrospective pilot study, 21 patients received coronary CTA. Subsequently a total of 32 vessels underwent invasive FFR measurement. For each vessel, FFR based on steady-state and analytical models (FFR_{SS} and FFR_{AM}, respectively) were calculated non-invasively based on CTA and compared with FFR. The accuracy, sensitivity, specificity, positive predictive value and negative predictive value were 90.6% (87.5%), 80.0% (80.0%), 95.5% (90.9%), 88.9% (80.0%) and 91.3% (90.9%) respectively for FFR_{SS} (and FFR_{AM}) on a per-vessel basis, and were 75.0%, 50.0%, 86.4%, 62.5% and 79.2% respectively for DS. The area under the receiver operating characteristic curve (AUC) was 0.963, 0.954 and 0.741 for FFR_{SS}, FFR_{AM} and DS respectively, on a per-patient level. The results suggest that the CTA-derived FFR_{SS} performed well in contrast to invasive FFR and they had better diagnostic performance than DS from CTA in the identification of functionally significant lesions. In contrast to FFR_{CT}, FFR_{SS} requires much less computational time.

Introduction

Coronary artery disease (CAD) is a very prevalent cardiovascular disease which can lead to angina and myocardial infarction (MI) [1–3]. The quantification of functional coronary stenosis is of high significance for patient management to prevent mortality from CAD [4].

Both anatomical parameters and hemodynamic indices are commonly applied to quantify the severity of CAD. The anatomical parameters of diameter stenosis (DS) and area stenosis (AS) express the diameter and area of a stenosed region, respectively, relative to a "normal" segment. Although computed tomography angiography (CTA) has proven valuable to characterize the anatomic severity of CAD with lower cost and fewer complications, it cannot determine the hemodynamic significance of a stenosis and it has high false positive rate in contrast to a hemodynamic index, such as fractional flow reserve, FFR [5]. FFR is defined as the ratio of maximal blood flow achievable in a stenotic artery to the theoretical maximal flow in the same vessel when stenosis is absent [6]. Assuming a linear pressure-flow relation, flow is proportional to pressure when resistance is constant. Therefore, FFR can be calculated as the ratio of the pressure distal to a coronary stenosis to aortic pressure at the hyperemia state [7]. Because FFR can identify the functionally significant coronary stenoses, including intermediate coronary stenoses [8–10], it is used as gold standard to identify those stenoses that can most likely benefit from percutaneous coronary intervention (PCI). Revascularization is commonly recommended when the coronary stenosis leads to FFR $\leq$ 0.80. FFR can only be measured via invasive coronary catheterization at hyperemic state, however, which carries higher medical cost and some complications [11]. There have been some alternative adoptions of FFR by either removing the need for adenosine [12] or pressure wire [13] but still require invasive angiography.

Recently, Computational Fluid Dynamics (CFD) has been applied to simulate blood flow to compute FFR_{CT} for patient-specific coronary artery models reconstructed from CTA, with lumped parameter heart and coronary models [14,15]. The multicenter clinical trials of DISCOVER-FLOW, DeFACTO and NXT [16–20] demonstrated that FFR_{CT}, derived non-invasively through combining CT images and CFD simulations, improved diagnostic accuracy and discrimination than CT alone in differentiating ischemic and non-ischemic stenoses. The computational time for transient CFD simulation, however, was significant (6 hours[16] or 1–4 hours [19] for CFD analysis per examination), which may limit its utility in the clinic. By modeling vessels as 1D segments in CFD simulation, the computational time was significantly reduced to 5–10 minutes per patient [21]. The latter approach, however, only had moderate to good correlation (Pearson correlation coefficient = 0.59) as compared with invasive FFR.

Since the calculation of FFR is based on time-averaged pressure measured over several cardiac cycles during coronary angiography [12], we hypothesize that non-invasive FFR_{SS} can be obtained from steady state flow simulation using novel boundary conditions while maintaining acceptable accuracy relative to FFR. In this way, the computational time can be reduced to 1/16 of the transit state model as reported in our previous study [22].

An alternative approach to CFD that yields real-time calculation is the use of analytical models. Huo et al. [23] recently proposed an analytical model to allow real-time computation of FFR_{AM}. The calculation of FFR_{AM} was based on stenosis dimensions (proximal, distal and minimal lumen area, and length) and hyperemic coronary flow rate through the lesion (i.e., no ad hoc or empirical parameters). This method has been validated in-vitro and in swine coronary arteries [23], but not clinically.

The aim of this pilot study was to compute FFR_{SS} and FFR_{AM} from CTA using steady state flow simulation and analytical model, respectively. The diagnostic performance of FFR_{SS} and FFR_{AM} was validated against the reference standard of invasive FFR.

Methods

Study Design

The pilot study was approved by the local institutional ethics review board (SingHealth CIRB 2014/363/C) and conducted in National Heart Centre Singapore. The informed consent was waived, as it is a retrospective study. Patient records/information was anonymized and de-identified prior to analysis. For inclusion in this retrospective study, coronary CTA must have been performed before coronary angiography due to clinical needs. Patients, who had undergone previous coronary interventions or coronary bypass surgery in the vessels of interest, and patients who had a cardiac event and/or PCI in between coronary CTA and invasive angiography were excluded from this study. Patients, who had Agatston coronary artery calcium score greater than 2,000 or non-diagnostic CTA image quality, were also excluded. From March 2010 to April 2013, 35 patients underwent CTA followed by invasive angiography with FFR. A total of 9 patients were excluded, 3 because of undergoing PCI in between CTA and invasive angiography, 5 because of Agatston coronary artery calcium score greater than 2,000, and 1 because of non-diagnostic CTA image quality. In total, 21 patients were recruited and their baseline characteristics were tabulated in Table 1. For the recruited patients, the time-lag between CTA and coronary angiography varied from 3 to 329 days with average time-lag of 48

Table 1. Baseline characteristics.

Variable (n = 21)	Mean ± SD or Frequency (%)
Age (years)	57 ± 10
Male	16 (76%)
Chinese	18 (86%)
Hypercholesterolemia	13 (62%)
Hypertension	11 (52%)
Diabetes	2 (10%)
Current smoker	2 (10%)
Previous percutaneous coronary intervention[+]	1 (5%)
Symptoms	
Chest Pain	9 (43%)
Shortness of Breath	7 (33%)
Laboratory measures	
Hemoglobin (g/dl)	13.6 ± 1.6
Hematocrit (%)	40.7 ± 4.3
Creatinine (μmol/L)	82.8 ± 15.8
Body-mass index (kg/m^2)	24.9±4.5
Medications	
Aspirin	13 (62%)
Beta-blocker	7 (33%)
Nitrate	5 (24%)
Statins	15 (71%)
ACE inhibitors	1 (5%)
Calcium-channel blockers	4 (19%)
Clopidogrel	4 (19%)
ARBs	5 (24%)

Notes: ACE represents angiotensin-converting enzyme, ARB represents angiotensin receptor blocker

[+] Not in the vessel territories interrogated with invasive FFR measurement.

doi:10.1371/journal.pone.0153070.t001

days. 81% of the recruited patients underwent CTA and coronary angiography within 50 days. The researchers were blinded to invasive FFR values before calculating the FFR_{SS} and FFR_{AM}.

Coronary CTA Acquisition

Standard coronary CTA was performed by using a 64 slice multi-detector CTA scanner (Toshiba Aquilion 64, 0.5mm × 64 detector row) in 1 (5%) patient (for patient #6 of Table 2) and a 320 slice multi-detector CTA scanner (Toshiba Aquilion ONE^{TM}, 0.5mm × 320 detector row) in the rest of 20 patients following current clinical guidelines [24]. The scanning range was planned individually to cover the major coronary arteries and aorta. Beta-blocker was administrated in 4 (19%) patients to moderate heart rate. Omnipaque non-Ionic contrast

Table 2. Invasive and non-invasive hemodynamic indices of patients with CAD.

Patient No	Location of Stenosis	FFR	FFR_{SS}	FFR_{AM}
1	LAD Mid	0.74	0.73	0.67
2	LAD Mid	0.83	0.87	0.93
3	LAD Mid	0.94	0.93	0.92
3	LAD D1	0.86	0.86	0.89
4	LAD Proximal	0.97	0.98	0.97
5	LAD Ramus	0.89	0.88	0.88
5	LAD D1	0.93	0.81	0.84
6	LAD Mid	0.78	0.78	0.69
7	R-PLB	0.71	0.72	0.85
8	RCA Distal	0.91	0.81	0.84
9	LAD Distal	0.73	0.73	0.64
9	LCX Mid	0.92	0.87	0.89
9	LCX OM1	0.95	0.84	0.95
10	LAD Mid	0.85	0.82	0.95
10	LAD D1	0.79	0.82	0.72
11	LAD Proximal	0.78	0.69	0.74
12	LAD Mid	0.83	0.88	0.88
13	LAD Mid	0.89	0.85	0.84
14	LAD Proximal	0.91	0.88	0.89
15	LAD Mid	0.85	0.75	0.78
16	RCA Mid	0.98	0.94	0.96
16	LAD Mid	0.81	0.81	0.79
16	LAD D2	0.63	0.67	0.51
17	RCA Proximal	0.95	0.85	0.87
18	LAD Mid	0.93	0.90	0.92
18	D1	0.92	0.92	0.91
18	RCA Mid	0.93	0.89	0.88
19	LAD Proximal	0.76	0.73	0.83
20	LAD Mid	0.86	0.87	0.88
20	LAD D1	0.84	0.84	0.94
21	LAD Mid	0.74	0.82	0.75
21	LAD Distal	0.66	0.67	0.47

Notes: LAD: left anterior descending artery; LCX: left circumflex artery
D1: first diagonal branch; R-PLB: right posterior descending artery
RCA: right coronary artery; OM1: first obtuse marginal branch.

doi:10.1371/journal.pone.0153070.t002

medium was routinely given before image acquisition to highlight regions of interest in the CT images. The dose of contrast was controlled by using electrocardiographic triggering prospectively. Image acquisition was performed with an inspiratory breath-hold. The scan parameters were gantry rotation time at 350–400 ms, tube potential at 100–120 kV and field of view (FOV) at 161–230mm. Depending on the cardiac dimensions and pitch, scanning time was 5.7–8.4 s for a single breath hold in the craniocaudal direction. All CT images were recorded with 0.25 mm increment (i.e., 0.5 mm slice thickness) and saved in 'DICOM' format' for image processing to reconstruct 3D patient-specific coronary models. The mean total Agatston coronary artery calcium score was 333±370 for the recruited patients.

Coronary Angiography and FFR Measurement

Coronary angiography was performed via percutaneous femoral approach according to standard guidelines [25]. For the recruited patients, invasive FFR measurement was performed due to clinical needs, according to the institutional protocol. Omnipaque non-Ionic contrast medium was routinely given during angiographic procedure to highlight the regions of interest. Pressure measurement was conducted in at least 1 vessel with pressure-sensor-tipped wire (RADI, Volcano or St Jude Medical pressure wire), followed by intravenous infusion (for patient #19 of Table 2 at dose of 60 μg/kg/min) or intracoronary bolus (for the rest 20 patients at dose of 60 to 200μg) of vasoactive substances (adenosine) to create maximal hyperemia. More patients underwent FFR measurements followed by intracoronary bolus injection of adenosine because of its advantages like shorter duration and better patient comfort. It has been reported, however, that intravenous infusion of adenosine yielded identical FFR result compared with intravenous infusion [26]. During maximum hyperemia, pressure measurements were repeated to calculate FFR. FFR $\leq$ 0.8 indicated a hemodynamically significant coronary stenosis.

Image Processing for Reconstructing Patient Specific Model

Image processing was performed to segment the artery structure from the background CT image for reconstructing the 3D coronary artery tree. At first, a Hessian matrix-based filter was applied to each single transverse CT image to obtain high order geometric characteristics; i.e., the principal curvature of image intensity [27]. Eigenvector analysis of the Hessian matrix obtained was used to determine whether the voxel under analysis belonged to the vessel structure or not. Finally, the graph-cuts based image segmentation technique [28] was applied to the enhanced 3D image, before using marching cube algorithm to establish the triangulated surface mesh from segmented voxel data. Manual editing was necessary for some models to remove artifacts and small vessels with diameters $<$ 1mm. This image processing algorithm has been previously validated [29].

Both AS and DS were calculated based on the reconstructed coronary artery tree model. AS (DS) was defined as 100% minus the percentage of minimal lumen area (diameter) to the reference lumen area (diameter) at the most appropriate reference site. The reference site was comprised of a non-diseased arterial segment in close proximity to the lesion, preferably with no intervening branch vessels [30]. As recommended in SCCT guideline [24], coronary stenoses can be graded as minimal (DS$<$25%), mild (25%$\leq$DS$\leq$49%), moderate (50%$\leq$DS$\leq$69%), severe (70%$\leq$DS$\leq$99%) and occlusion (DS = 100%) stenoses separately. Following the guideline, a stenosis with DS $\geq$ 50% was considered as an anatomically significant stenosis. Although AS was believed to be more accurate and less dependent on the projection plane and reference site than DS [30], there are only a few studies on its reproducibility and accuracy. As suggested by a recent study [31], AS $\geq$ 62% was used as a threshold to identify the ischemic coronary lesions.

CFD Simulation to Derive FFR_{SS}

ANSYS workbench, a commercial software, was used to discretize the computational domain into tetrahedral shaped elements. After mesh dependency test, the coronary artery tree model was discretized with a total of about 0.8 million volume cells. Further grid refinement led to $< 1\%$ relative error in maximum velocity.

FLUENT^{TM} was used to solve continuity and Navier-Stokes equations. Blood was modeled as Newtonian fluid to simulate blood flow in the patient-specific coronary artery tree models. Appropriate boundary conditions were specified at the inlet and outlets of each model respectively to mimic physiological conditions (see details in S1 Appendix), and satisfy 3 key principles, which were also applied in [16,19]. First, coronary supply was assumed to meet myocardial demand at rest. Hence, resting total coronary blood flow rate can be calculated from myocardial mass which were assessed from CT images [32,33]. Second, the resistance of each coronary branch at rest was proportional to the size of parent and child branch vessels [34]. Third, coronary resistance was assumed to reduce predictably during hyperemia conditions (see details in S1 Appendix), which was within the physiological range measured by Wilson et al. [35].

In contrast to previous studies [16,19], steady flow simulation with a novel iterative boundary condition was employed in this study, which reduced the computational cost significantly in contrast to using pulsatile flow simulation. All computations were executed in a Dell T7500 workstation and it took 0.5 to 2 hours of computational time for one case. The computational time could be further reduced with more advanced hardware.

Analytical Calculation to Obtain FFR_{AM}

Huo et al. [23] proposed an analytical model to predict FFR based on stenosis dimensions and hyperemic coronary flow with no empirical parameters, which has been validated in-vitro and in vivo in swine. We used this model for calculating FFR_{AM} for human data. The analytical model was derived from energy conservation which considered the convection and diffusive energy losses as well as the energy loss due to sudden constriction and expansion in lumen area. In this study, the hyperemic coronary flow rate through the coronary branches was specified with the data obtained from simulation. Together with the dimensions (proximal, distal and minimal lumen area, and length) of the stenosis, the pressure drop over a stenosis (ΔP_1) was derived according to the analytical model (see S2 Appendix). The pressure drop over the normal vessel segments (from the inlet to the segment before stenosis), ΔP_2, was calculated according to Poiseuille equation. Accordingly FFR_{AM} was calculated by $1-(\Delta P_1+\Delta P_2)/P$ where P represented patient-specific mean aortic pressure. In this way, FFR_{AM} was computed real-time.

Statistical Analysis

To assess the diagnostic performance of FFR_{SS} and FFR_{AM}, the clinical standard ($FFR \leq 0.8$) was used as a reference. A patient was considered positive if any vessel had $FFR \leq 0.8$. The same threshold (0.8) was applied for both FFR_{SS} and FFR_{AM}. To compare with the diagnostic performance of CTA, $DS \geq 50\%$ [30] and $AS \geq 62\%$ [31] were used as the threshold to identify the ischemic lesions in this study. For statistical analysis, all continuous variables were reported as means ± standard deviations and absolute variables were presented as totals or percentages. Pearson correlation coefficient, Bland-Altman analysis and the area under the receiver-operating characteristic curve (AUCs) were calculated to determine the correlations, differences and diagnostic performance of variable indicators, respectively. All statistical analyses were performed using SPSS version 16.0 and MedCalc version 16.2.1.

Results

Patient Characteristics

Table 1 shows the baseline characteristics of the study cohort. As a pilot study, 21 patients (aged 57±10 years, 16 males and 5 females) underwent CTA and invasive angiography tests; 43% of patients had chest pain, while 33% had shortness of breath. There were no adverse events or revascularization between the tests. FFR was invasively measured in a total of 32 coronary vessels (as shown in Table 2) where 84% (n = 27) of the stenosed vessels were located in the left coronary artery tree. Of the 32 vessels, the invasively measured FFR was 0.85±0.09 and 31% (n = 10) of the vessels had functionally significant stenoses (FFR≤0.8). The SYNTAX score [36] was 2 to 34.5 for the recruited patients with a mean value of 11.3.

Assessment of Functional Significance of Coronary Artery Stenosis

A 3D coronary artery tree was reconstructed from CTA images through image processing. An example of CTA images is shown in Fig 1A where the stenoses were observed along the left

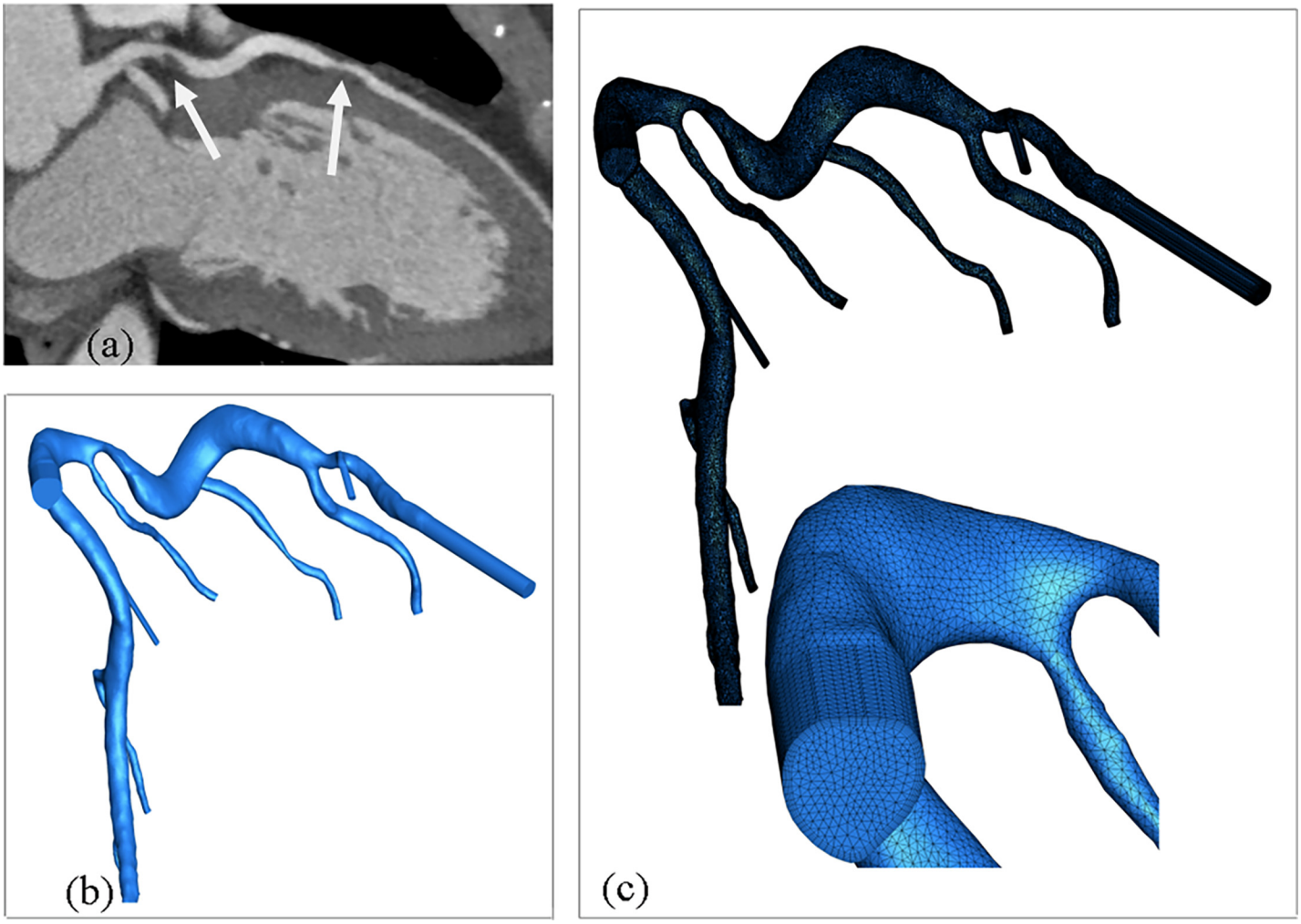

Fig 1. (a) Coronary CTA images for a 52-years-old man, which showed two stenoses (indicated by white arrows) along the left anterior descending artery (b) 3D coronary model reconstructed from CTA images and (c) meshes generated for this model with enlarged view of dense meshes assigned near the wall.

doi:10.1371/journal.pone.0153070.g001

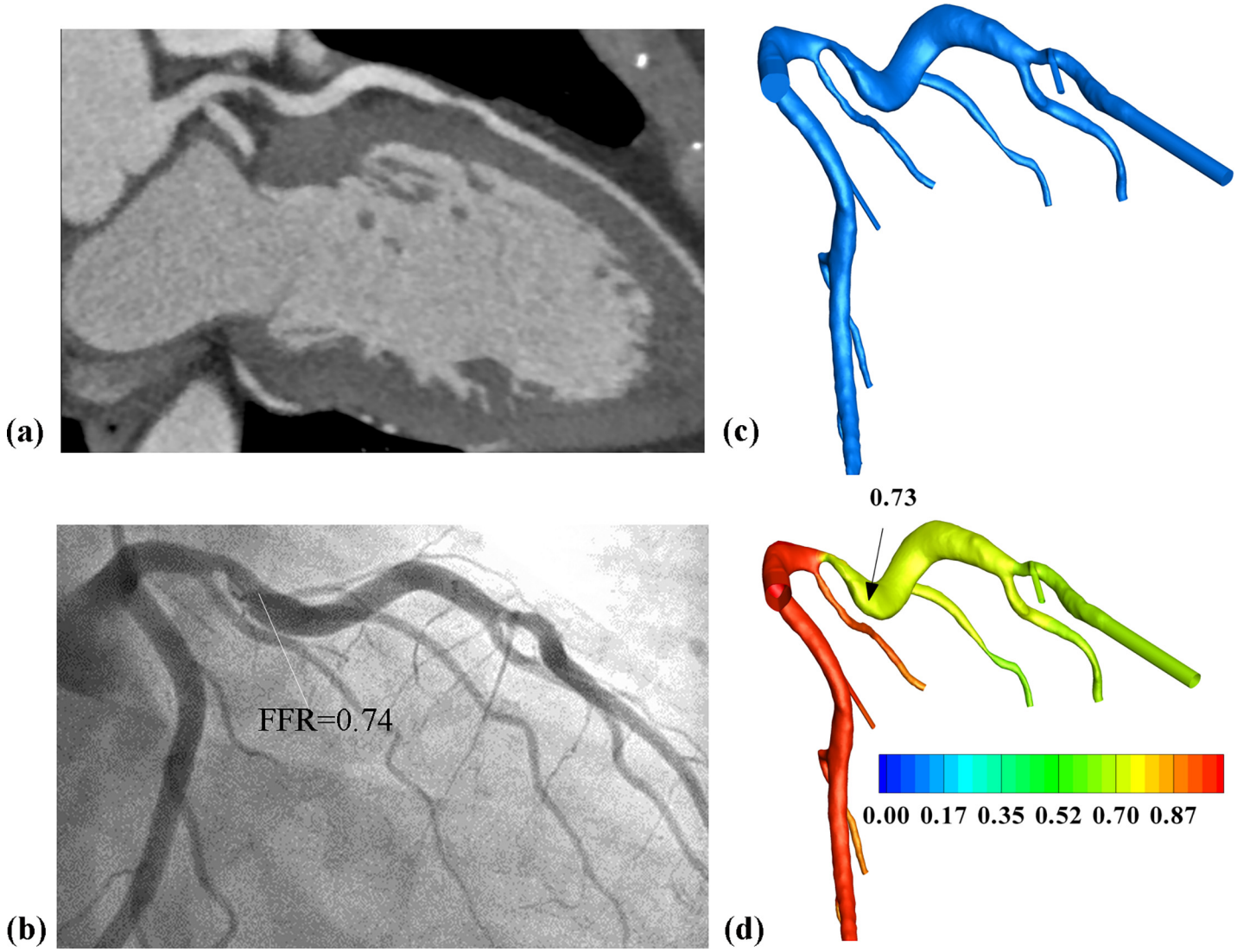

Fig 2. Representative patient with functional significant stenosis. Severe luminal stenosis was observed from (a) CTA images and (b) invasive angiography measured FFR at 0.74 (FFR≤0.8). Based on the (c) 3D model reconstructed from CTA images, CFD derived (d) pressure distributions on the 3D model and the calculated FFR_{SS} was 0.73.

doi:10.1371/journal.pone.0153070.g002

anterior descending artery (LAD). The reconstructed model showed that the coronary lumens were far from circular in the stenotic regions. Meshes were generated (Fig 1C) for the 3D model to facilitate CFD iterations. In this way, CTA-derived non-invasive FFR_{SS} can be calculated.

Two representative examples are shown in Figs 2 and 3 separately. Based on CTA, severe (Fig 2A) and moderate (Fig 3A) stenoses were observed for two patients, respectively. One stenosis turned out to be functionally significant (Fig 2B) while the other non-significant (Fig 3B) with measured FFR of 0.74 and 0.97, respectively. Based on the CTA-derived CFD, the pressure distributions were calculated on these two models and the calculated FFR_{SS} were 0.73 and 0.98, respectively. Using the analytical model, the calculated FFR_{AM} were 0.67 and 0.97 separately for these two stenoses.

Table 2 tabulates both hemodynamic indices obtained through invasive angiography and those derived non-invasively from CTA. Fig 4A and 4B show the correlation of FFR_{SS} and

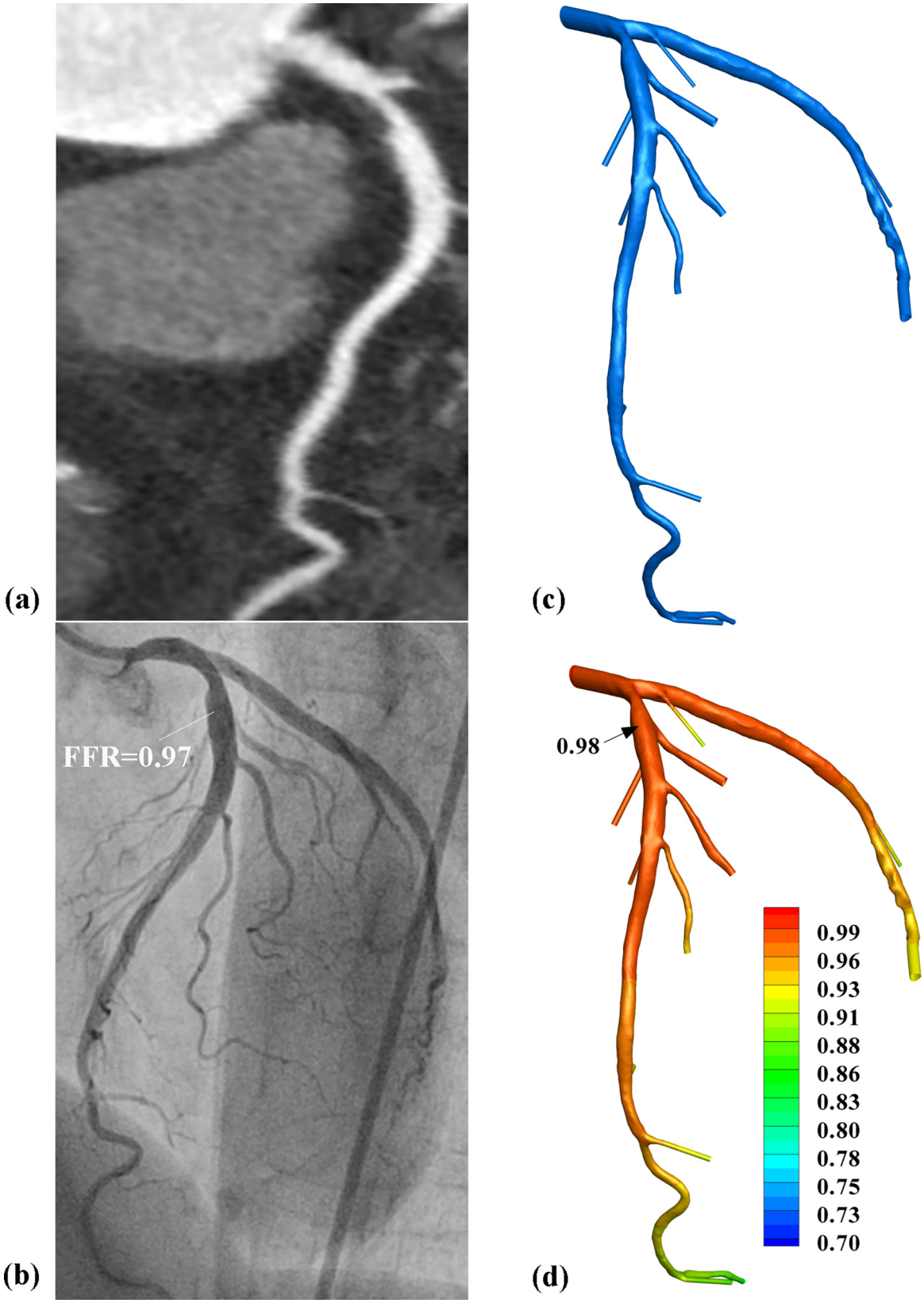
(a)
(b)
FFR=0.97
(c)
(d)
0.98
0.99
0.96
0.93
0.91
0.88
0.86
0.83
0.80
0.78
0.75
0.73
0.70

Fig 3. Representative patient with functional non-significant stenosis. Moderate luminal stenosis was observed from (a) CTA images and (b) invasive angiography measured FFR at 0.97 (FFR>0.8). Based on the (c) 3D model reconstructed from CTA images, CFD derived (d) pressure distributions on the 3D model and the calculated FFR_{SS} was 0.98.

doi:10.1371/journal.pone.0153070.g003

FFR_{AM} with FFR, respectively. Both FFR_{SS} (Pearson's correlation coefficient 0.843, $p<0.001$) and FFR_{AM} (Pearson's correlation coefficient 0.825, $p<0.001$) showed strong correlation with FFR. Both FFR_{SS} (mean difference 0.026, standard deviation 0.050, Fig 5A) and FFR_{AM} (mean difference 0.016, standard deviation 0.066, Fig 5B) demonstrated slight but non-significant differences as compared with FFR in assessing the functional significance of stenosis on a per-vessel basis.

Diagnostic Performance of AS, DS, FFR_{SS} and FFR_{AM} for Diagnosis of Ischemia

In contrast to the gold standard of FFR, CTA-derived hemodynamic indices of FFR_{SS} (AUC was 0.955 and 0.963 on a per-vessel and per-patient basis, respectively) and FFR_{AM} (AUC was 0.968 and 0.954 on a per-vessel and per-patient basis, respectively) have higher AUC than AS (AUC was 0.818 and 0.880 on a per-vessel and per-patient basis respectively) and DS (AUC was 0.709 and 0.741 on a per-vessel and per-patient basis respectively) measured from CTA on both per-vessel (Fig 6A) and per-patient (Fig 6B) bases. The difference between AUCs of FFRss and DS was significant ($p<0.05$) on both per-vessel and per-patient bases.

By combining CTA with steady state flow simulation and analytical models separately, the diagnosis accuracy of both FFR_{SS} (90.6%) and FFR_{AM} (87.5%) was higher than that of anatomical index of either AS (75.0%) or DS (75.0%) from CTA alone, on a per-vessel basis (Table 3). Higher specificity was found for CTA-derived FFR_{SS} (95.5%) than AS (72.7%) and DS (86.4%) derived from CTA alone, with the same (in contrast to AS) or improved (in contrast to DS) sensitivity, which were 80.0%, 80.0% and 50.0% respectively on a per-vessel basis. CTA-derived hemodynamic index (either FFR_{SS} or FFR_{AM}) was found to enhance both PPV and NPV than CTA-based anatomic index (either DS or AS) on a per-vessel basis. The enhancement of diagnostic performance by replacing anatomic index of either DS or AS to CTA-derived hemodynamic index (either FFR_{SS} or FFR_{AM}) was also found on a per-patient basis (Table 3).

Effect of Individual Hyperemic Response on the Calculated FFR_{SS}

To investigate the effects of individual hyperemic response on the calculated FFR_{SS}, we carried out a series of numerical simulations on a single patient-specific model and varied the values of K. It was found that FFR_{SS} increased with increasing K (Fig 7). With K ranging from 0.16 to 0.36 (within physiological hyperemia response range [35]), the maximum variation of FFR_{SS} was less than 2.4%, compared to the FFR_{SS} value obtained at K = 0.21.

Discussion

Non-invasive Assessment of Anatomic Significance of Stenosis using CTA

As a non-invasive examination, CTA is used to characterize the anatomic severity (DS and AS) of CAD with fair medical cost and less complications than invasive procedures. In this study, the anatomic parameters of DS and AS were measured for each stenosis of patient-specific model reconstructed from CTA images. The inter-operator variability of DS (5.6%) was higher than AS (1.5%). This is because the determination of DS is somewhat subjective, owing to the difficulty of delineating both stenotic and normal reference segments under multiple

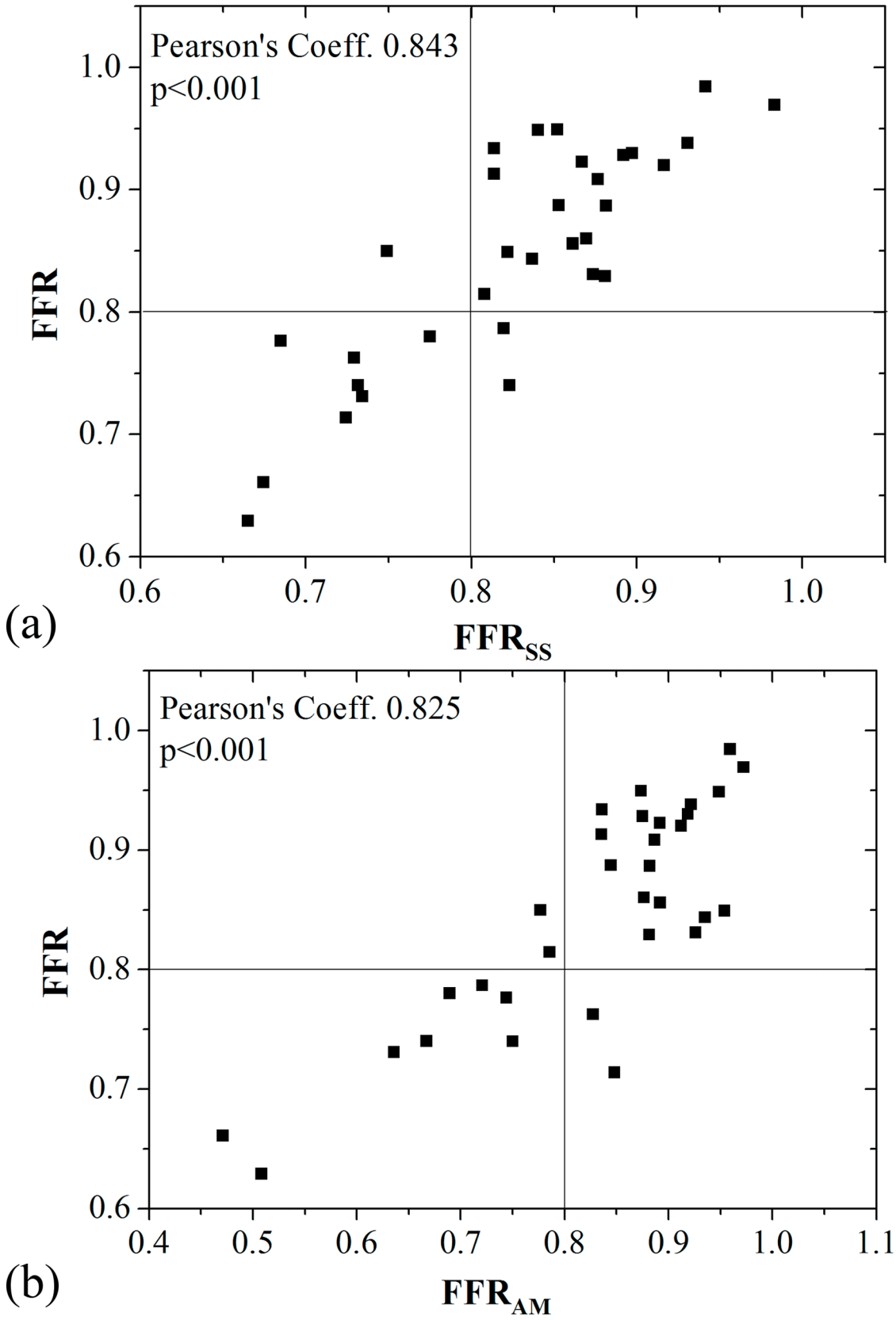

Fig 4. Correlation between FFR with (a) FFR_{SS} and (b) FFR_{AM} for a total of 32 stenoses.

doi:10.1371/journal.pone.0153070.g004

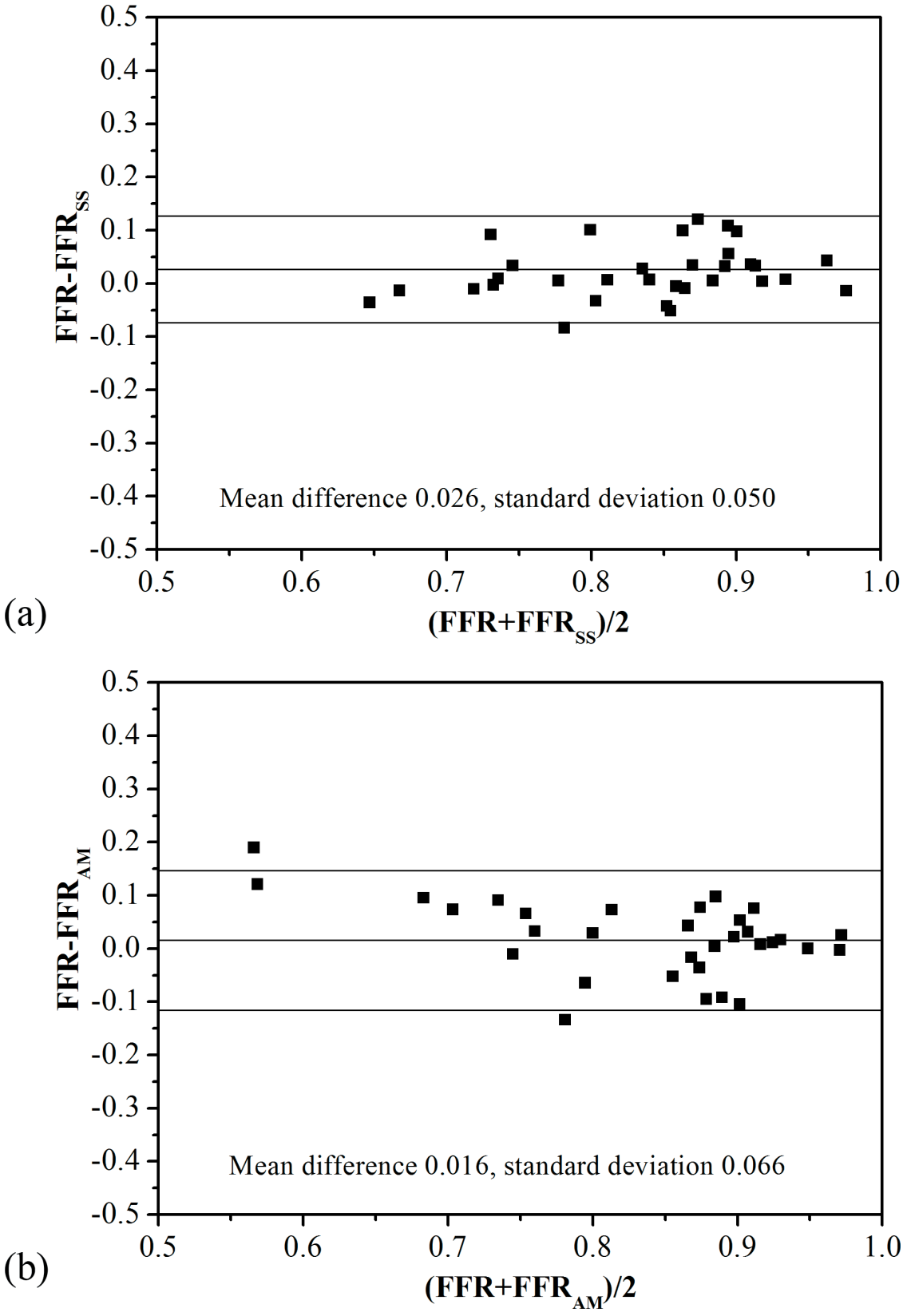

Fig 5. Bland-Altman plot of (a) FFR with FFR_{SS} and (b) FFR with FFR_{AM} on a per-vessel basis.

doi:10.1371/journal.pone.0153070.g005

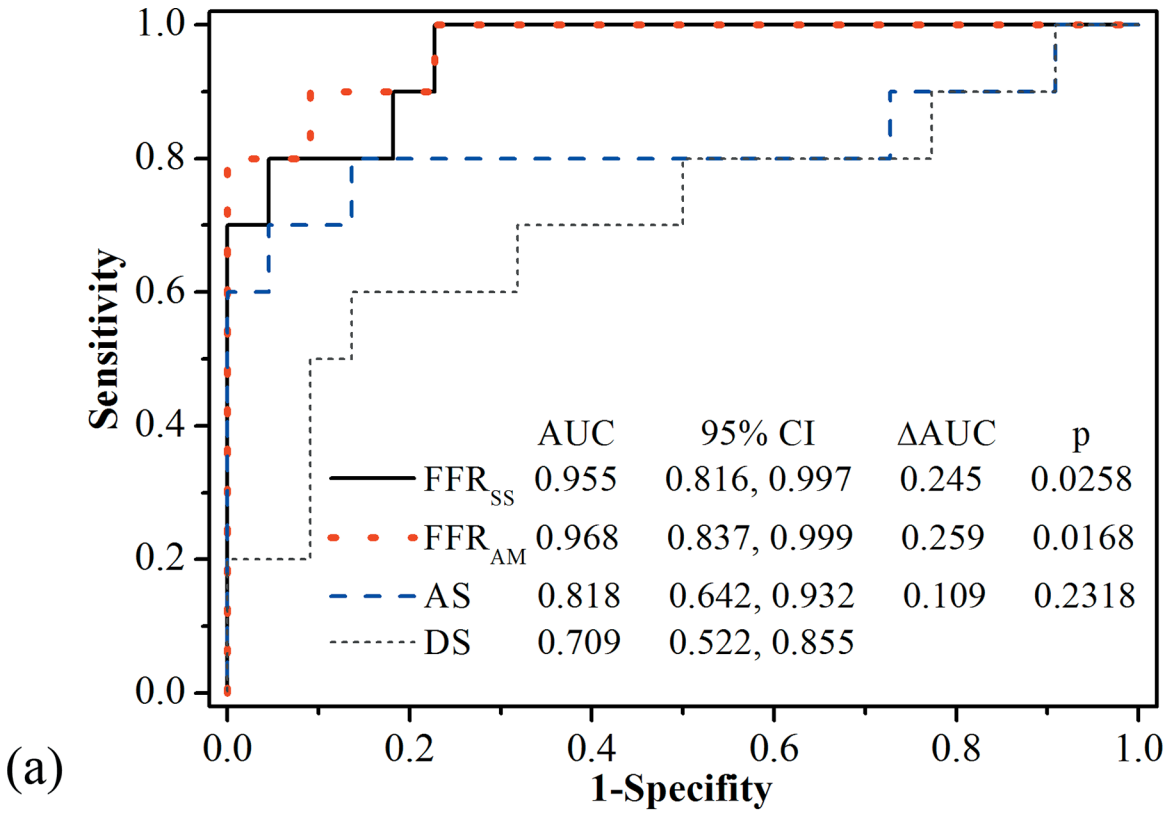
Sensitivity
1-Specifity
AUC 95% CI ΔAUC p
FFR_SS 0.955 0.816, 0.997 0.245 0.0258
FFR_AM 0.968 0.837, 0.999 0.259 0.0168
AS 0.818 0.642, 0.932 0.109 0.2318
DS 0.709 0.522, 0.855

(a)

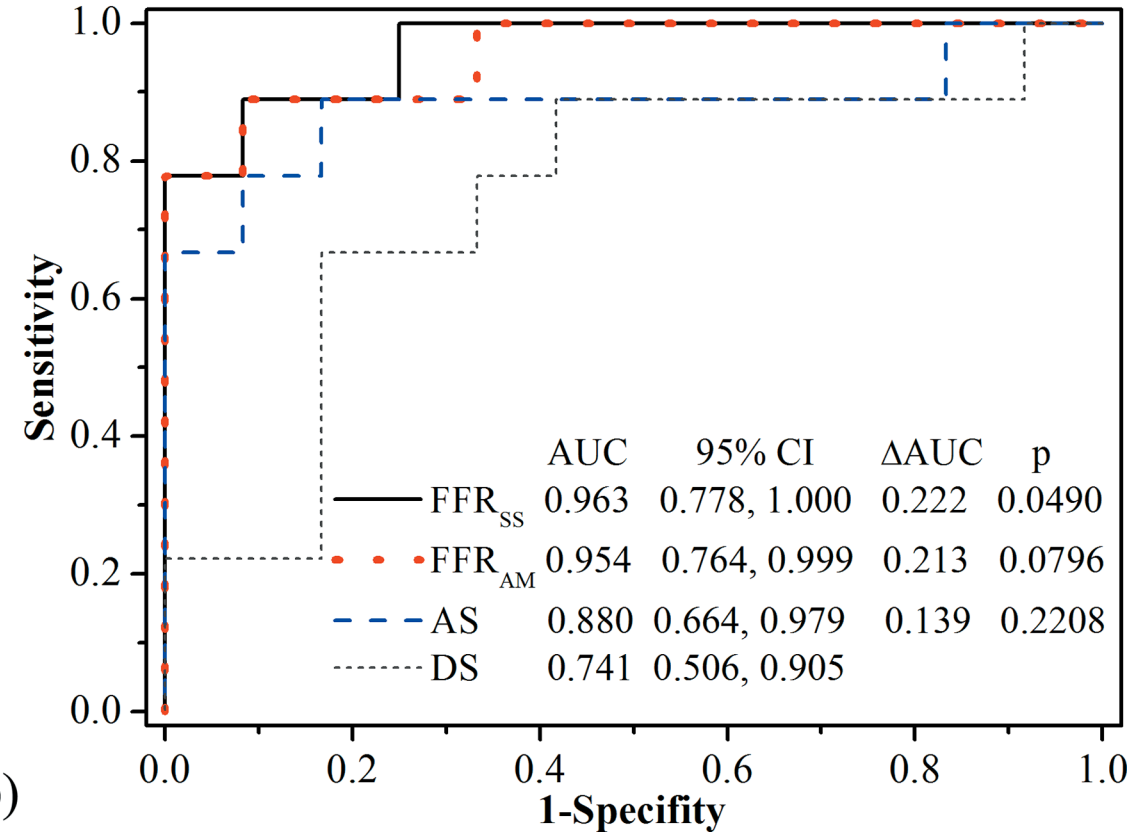
Sensitivity
1-Specifity
AUC 95% CI ΔAUC p
FFR_SS 0.963 0.778, 1.000 0.222 0.0490
FFR_AM 0.954 0.764, 0.999 0.213 0.0796
AS 0.880 0.664, 0.979 0.139 0.2208
DS 0.741 0.506, 0.905

(b)

Fig 6. Area under the receiver-operating characteristic curve (AUC) of FFR_{SS}, FFR_{AM}, AS and DS and the difference between AUCs of FFR_{SS} (FFR_{AM} and AS) and DS for discriminating ischemic stenosis on a (a) per-vessel and (b) per-patient basis separately.

doi:10.1371/journal.pone.0153070.g006

pathological states (e.g., diffuse CAD, high-flow coronary fistulae and ectasia). In contrast to DS, AS had less dependency of projection plane and reference sites [30].

As anatomical measures, DS and AS measured from CTA cannot characterize the hemodynamic and functional significance of CAD on myocardial blood supply. In this study, 8 vessels were found to have DS $\geq$ 50%, while only 5 vessels led to FFR $\leq$ 0.8. This is consistent with the findings that using the anatomic index of DS to diagnose ischemia in stenosis leads to a much higher false positive rate relative to FFR [37]. These results appear to confirm the clinical findings [5,37] that DS tends to overestimate the significance of stenosis for ischemia [38,39].

In contrast to DS (AUC was 0.709 and 0.741 on a per-vessel and per-patient basis separately), AS better (but not significant, $p>0.05$) discriminated non-ischemic and ischemic groups (AUC was 0.818 and 0.880 on a per-vessel and per-patient basis separately). This was because the pressure drop over a stenotic region was largely attributed to convective and diffusive energy losses due to constriction and sudden expansion of the lumen area distal to the stenosis [23]. The accuracy of AS was limited (75.0% on a per-vessel basis), however, due to the difficulty to delineate both the stenotic and the normal reference segments under many pathological states (such as diffuse CAD, high-flow coronary fistulae, ectasia, etc.), the limitations of imaging resolution, the effects of stenosis location and length of the stenosis, exit angle, and other physiological factors on the hemodynamics of CAD [40].

Non-invasively Assessment of Hemodynamic Significance of Stenosis via FFR_{SS}

In this study, FFR_{SS} was obtained non-invasively by combining steady state flow simulation with CTA images. The novel specification of boundary conditions greatly reduced the

Table 3. Diagnostic performance of FFR_{SS}, FFR_{AM}, AS and DS compared to invasively measured FFR for discrimination of ischemic coronary stenosis (ischemic group, FFR$\leq$0.8; non-ischemic group, FFR>0.8)

	Criterion to discriminate ischemic stenosis	Accuracy (%)	Sensitivity (%)	Specificity (%)	PPV (%)	NPV (%)
Per-vessel	FFR_{SS} $\leq$0.8 (95% CI)	90.6 (75.0–98.0)	80.0(44.4–97.5)	95.5 (77.2–99.9)	88.9 (51.8–99.7)	91.3 (72.0–98.9)
	$FFR_{AM}\leq$0.8 (95% CI)	87.5 (71.0–96.5)	80.0 (44.4–97.5)	90.9 (70.8–98.9)	80.0 (44.4–97.5)	90.9 (70.8–98.9)
	AS$\geq$62% (95% CI)	75.0 (56.6–88.5)	80.0 (44.4–97.5)	72.7 (49.8–89.3)	57.1 (28.9–82.3)	88.9 (65.3–98.6)
	DS$\geq$50% (95% CI)	75.0 (56.6–88.5)	50.0 (18.7–81.3)	86.4 (65.1–97.1)	62.5 (24.5–91.5)	79.2 (57.9–92.9)
Per-patient	FFR_{SS} $\leq$0.8 (95% CI)	90.5 (69.6–98.8)	88.9 (51.8–99.7)	91.7 (61.5–99.8)	88.9 (51.8–99.7)	91.7 (61.5–99.8)
	$FFR_{AM}\leq$0.8 (95% CI)	85.7 (63.7–97.0)	77.8 (40.0–97.2)	91.7 (61.5–99.8)	87.5 (47.4–99.7)	84.6 (54.6–98.1)
	AS$\geq$62% (95% CI)	76.2 (52.8–91.8)	80.0 (44.4–97.5)	72.7 (39.0–94.0)	72.7 (39.0–94.0)	80.0 (44.4–97.5)
	DS$\geq$50% (95% CI)	71.4 (47.8–88.7)	55.6 (21.2–86.3)	83.3 (51.6–97.9)	71.4 (29.0–96.3)	71.4 (41.9–91.6)

PPV: Positive Predictive Value; NPV: Negative Predictive Value; CI: Confidence Interval.

doi:10.1371/journal.pone.0153070.t003

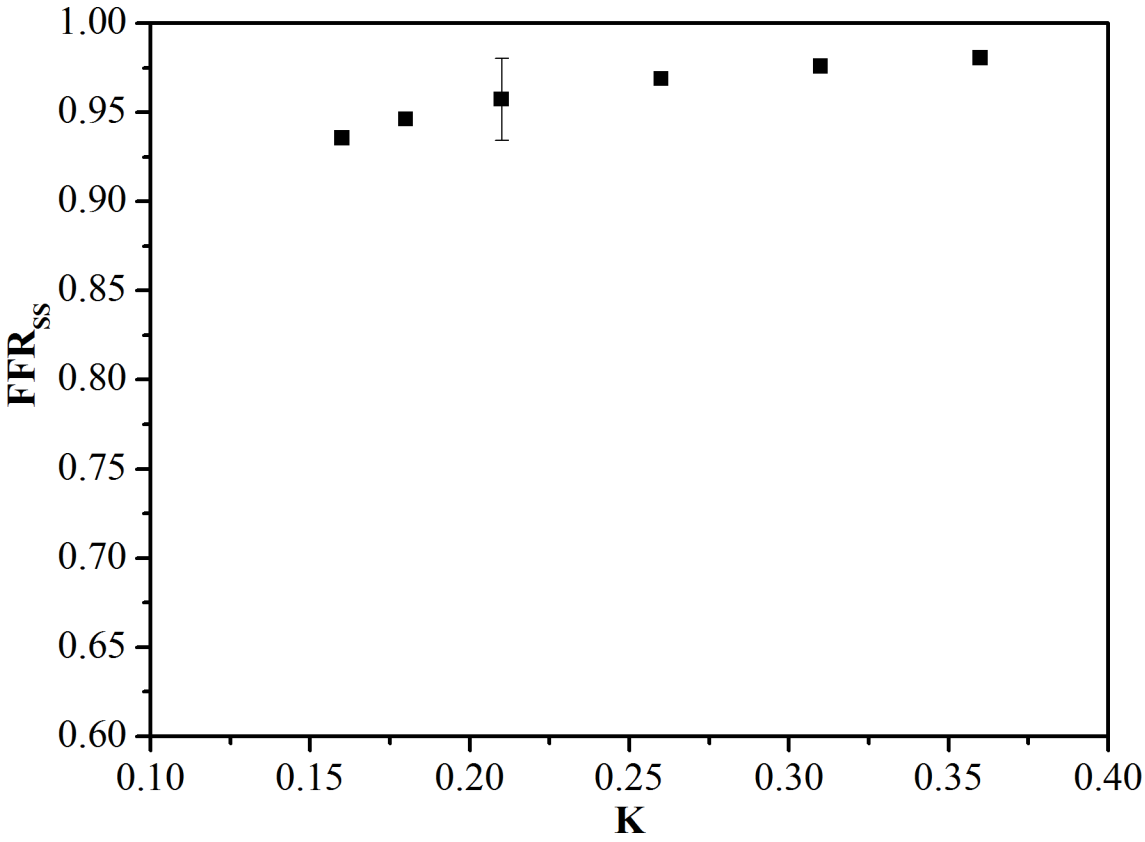

Fig 7. Sensitivity of FFR_{SS} with a varied K.

doi:10.1371/journal.pone.0153070.g007

computational time as compared to those of pulsatile flow simulations [22]. The pulsatile flow simulations were used to compute FFR_{CT} for the trials of DISCOVER-FLOW [16], DeFACTO [18] and NXT [19] and it took 6 hours [16] or 1–4 hours [19] for CFD analysis per examination. Direct comparison of the computational time between FFR_{CT} trials and current study is not practical, as the hardware specifications of the workstations [16,18,19] was not known. Our previous study showed that the computational time with steady flow simulation was only 1/16 time of that in pulsatile flow simulation [22], using the same workstation, which demonstrated the significant reduction of computational time with our proposed approach.

In this pilot study, FFR_{SS} was found to have very high diagnostic performance in contrast to invasively measured FFR. The correlation between FFR_{SS} and FFR in this study (Pearson's correlation coefficient 0.843, $p<0.001$) was equivalent with that of NXT (Pearson's correlation coefficient 0.82, $p<0.001$), DeFACTO (Pearson's correlation coefficient 0.63) and Discover-Flow (Pearson's correlation coefficient 0.72) trials. Similar level of the accuracy and AUC (on a per-patient basis) in this study (90.6% and 0.955 respectively) was observed in contrast to those of NXT (81% and 0.90 respectively), DeFACTO (73% and 0.81 respectively) and Discover-Flow (87.4% and 0.92 respectively) trials.

The slight improvement of correlation, accuracy and AUC in this study may be due to the two reasons. First, it may be attributed to the improvement of CT image quality. In this study, the majority of the patients (n = 20, 95%) received CTA examination with a 320 slice Toshiba Aquilion ONE^{TM} CT scanner and 1 patient with 64 slice multi-detector CTA scanner (Toshiba Aquilion 64) in the same center. CTA was performed using CTA scanners, however, with a minimum of 64 detector rows in multiple centers for NXT trial [19]. The CTA scanner

information was not provided in [19], but the scanners were listed as LightSpeed VCT/Discovery from GE, SOMATOM Sensation and Definition from Siemens, Brilliance 256 and 64 from Philips, Aquilion ONE and 64 from Toshiba in [41] for DeFACTO trial. Because Toshiba Aquilion CT scanners have finer detector elements of 0.5 mm than many other CT scanners (GE LightSpeed VCT: 0.625mm; Siemens Sensation 64: 0.6mm; Philips Brilliance 64: 0.625mm), the scanner used in this pilot study might have higher image resolution than some of the centers participating in the NXT trial and the image quality may have been better and more consistent. This finding was in agreement with NXT trial, which reported that the enhancement of diagnostic performance of FFR_{CT} was related to the increased CT image quality, comparing with the trials of DISCOVER-FLOW [16] and DeFACTO [18]. Second, it may be due to the consistent CTA protocol and imaging processing techniques applied in our center, which minimize the propagation of anatomic structure variations into the errors of FFR_{SS}.

A recent study attempted to reduce the computational time to 5–10 minute per patient but found a moderate (Pearson's correlation coefficient 0.59) correlation between their calculated FFR and invasive FFR [21]. Although the poor correlation may be due, in part, to higher Agatston coronary calcium score (555±542) in their study than our study (333 ±370), their method to simplify the flow in 3D vessel as 1-D flow may lead to oversimplification of coronary blood flow mechanics and results in significant error in the CTA-derived FFR calculation.

Non-invasive Analytical Assessment of Hemodynamic Significance of Stenosis via FFR_{AM}

In this pilot study, the hemodynamic index of FFR_{AM} was found to have good diagnostic performance when compared with the gold standard of FFR. The correlation between FFR_{AM} and FFR was high (Pearson's correlation coefficient 0.825, $p<0.001$). Based on Bland-Altman plot (Fig 5B), there was no significant difference between FFR_{AM} and FFR (mean difference 0.016). In contrast to FFR_{CT} (Pearson's correlation coefficient was 0.63 to 0.82 [16,18,19]), FFR_{AM} had closer correlation with FFR (0.83 separately). Equivalent accuracy of FFR_{AM} in this study (87.5% for per-vessel analysis) was also observed in contrast to those of FFR_{CT} studies (84.3% to 86% for per-vessel analysis) [16,18,19]. Therefore, the analytical model [23] has potential to predict myocardial FFR. Although the diagnostic performance of FFR_{AM} (AUC = 0.95) was slightly worse than FFR_{SS} (AUC = 0.96) for per-patient analysis, the real time calculation (negligible computational time) is an advantage.

The discrepancy between FFR_{AM} and FFR_{SS} may be due to the simplification of the analytical model. The former was largely dependent on the measurement of stenosis dimensions (proximal, distal and minimal lumen area, and length) and hyperemic coronary flow rate through the lesion. It is worth noting that the hyperemic coronary flow rate used in this study was from the numerical simulation. Since coronary angiography can quantify coronary blood flow [42,43], the analytical formulation has utility in angiography or in future developments of fast CTA, echocardiography or magnetic resonance angiography that may provide simultaneous coronary images and flow rate.

Limitations of the Study

This study has several limitations. First, the computational models may not capture the tremendous biological variability between CAD patients. For example, FFR is measured by pressure wire at the hyperemia state. Wilson et al. [35] reported that the total coronary resistance was reduced from 0.16 to 0.36 (K) times its resting value following an intracoronary adenosine bolus of 16μg (intracoronary adenosine infusion at 120–240 μg/min or intravenous adenosine infusion at 140 μg/kg/min). We found that FFR_{SS} increased with increasing K. This was

because higher downstream vascular resistance led to a reduction in the flow and pressure drop over the stenosis, resulting in higher FFR_{SS}. Within physiological hyperemia response range [35] (K ranging from 0.16 to 0.36), the maximum variation of FFR_{SS} was less than 2.4%, compared to the FFR_{SS} value obtained at $K = 0.21$. Therefore, FFR_{SS} was not particularly sensitive to the individual hyperemic response in patients free of microvascular disease. The assumption of normal microvascular function is one of the limitations of this study. Our recruited patients have no prior myocardial infarction (MI) or PCI in the vessel territories interrogated with invasive FFR measurement, however, which implies that their microvascular dysfunction is minimal. Furthermore, only 2 patients presented diabetes. The assumption of normal microvascular function was also applied to other non-invasive FFR studies [16,17,20]. The diagnostic performance of FFR_{SS} can be further examined in a myriad of patient cohorts [44], including those patients with left ventricular hypertrophy, diabetic (with increased fibrosis), prior MI or PCI, who may display important differences in microvascular resistance.

Second, the simulations assumed the coronary artery vessels as rigid and did not consider the motion of compliant vessel wall and the heart during the cardiac cycle. The movement of the heart and compliant vessel walls was reported to be less important, however, in coronary arteries than the geometry and boundary conditions on the pressure and flow fields [45,46].

Third, only time-averaged flow patterns and pressure distributions were predicted by the steady state flow simulation in this study. Although the deduced FFR_{SS} was comparable to FFR measured with pressure wire, detailed pulsatile flow simulation as in [20] will be necessary if transient pressure waveforms are of interest.

Fourth, although the addition of FFR_{SS} to coronary CTA is possible, adoption of FFR_{SS} in clinical domain remains challenging in view of the following: 1) inherently lower diagnostic accuracy of intermediate stenosis, when FFR is close to the cut point, even for the repeated invasive measurement of FFR [47] and 2) necessary introduction of a number of physiological assumptions for CFD. Therefore, additional investigations on larger appropriately designed prospective trials are necessary to provide more definitive data.

Finally, this is a single center study. The sample size was relatively small and the patients with previous coronary intervention were excluded. Further study on a larger population with wider recruitment criteria is necessary to verify and expand the present findings.

Significance

Although non-invasively derived FFR from CTA images has been attempted by several groups, it may lead to long computational times [16,18,19] or moderate accuracy [21]. A major contribution of our study is a steady flow simulation algorithm that can reduce the computational burden [13] to 1/16 compared with pulsatile flow simulation [22] but maintains high accuracy in relation to FFR (Pearson's correlation coefficient 0.843 ($p<0.001$) for FFR_{SS} and 0.82 ($p<0.001$) for FFR_{CT} [19]). An additional contribution is the clinical validation of an analytical model for deriving FFR_{AM} in real time. These simplified models that maintain accuracy may add to the current developments of non-invasive measurements of FFR for diagnosis of intermediate CAD lesions.

Supporting Information

S1 Appendix.
(DOCX)

S2 Appendix.
(DOCX)

Acknowledgments

The authors acknowledge the support of all staff at National Heart Centre Singapore, especially Fong Chin Teck, Yvonne Ng Kiat Hian, Max Wu Bing Huang, Ho Pei Yi and the staffs in the catheter laboratory and CT departments.

Author Contributions

Conceived and designed the experiments: JMZ LZ RST. Performed the experiments: JMZ TL AML. Analyzed the data: JMZ LZ YH GSK JY. Contributed reagents/materials/analysis tools: JMZ TL YH MW. Wrote the paper: JMZ LZ RST JCA GSK. Data Collection: JMZ AML STL ASLW JWCT KKY JMF FYJK MW BS XZ TSJC SYT JY.

References

1. Heidenreich PA, Trogdon JG, Khavjou OA, Butler J, Dracup K, Ezekowitz MD, et al. Forecasting the future of cardiovascular disease in the United States: A policy statement from the American Heart Association. Circulation. 2011; 123: 933–944. doi: 10.1161/CIR.0b013e31820a55f5 PMID: 21262990
2. Singapore I& CA (ICA). Registry of births and deaths 2011. Singapore Demogr Bull. 2012;
3. Roger VL, Go AS, Lloyd-Jones DM, Adams RJ, Berry JD, Brown TM, et al. Heart disease and stroke statistics-2011 update: A report from the American Heart Association. Circulation. 2011; 123:e18–e209. doi: 10.1161/CIR.0b013e3182009701 PMID: 21160056
4. Fihn SD, Blankenship JC, Alexander KP, Bittl J A, Byrne JG, Fletcher BJ, et al. 2014 ACC/AHA/AATS/PCNA/SCAI/STS focused update of the guideline for the diagnosis and management of patients with stable ischemic heart disease. Circulation.2014; 130: 1749–1767. doi: 10.1161/CIR.0000000000000095 PMID: 25070666
5. Meijboom WB, Meijs MFL, Schuijf JD, Cramer MJ, Mollet BR, van Mieghem CAG, Nieman K, van Werkhoven JM, Pundziute G, Weustink AC, de Vos AM, Pugliese F, Rensing B, Jukema JW, Bax JJ, Prokop M, Doevendans PA, Hunink MGM, Krestin GP de FP. Diagnostic accuracy of 64-slice computed tomography coronary angiography. J Am Coll Cardiol. 2008; 52: 2135–2144. doi: 10.1016/j.jacc.2008.08.058 PMID: 19095130
6. Spaan JAE, Piek JJ, Hoffman JIE, Siebes M. Physiological basis of clinically used coronary hemodynamic indices. Circulation. 2006; 113: 446–55. doi: 10.1161/CIRCULATIONAHA.105.587196 PMID: 16432075
7. Rajani R, Wang Y, Uss A, Perera D, Redwood S, Thomas M, et al. Virtual fractional flow reserve by coronary computed tomography—hope or hype? EuroIntervention. 2013; 9: 277–84. doi: 10.4244/EIJV9I2A44 PMID: 23793012
8. De Bruyne B, Pijls NHJ, Kalesan B, Barbato E, Tonino P a L, Piroth Z, et al. Fractional flow reserve-guided PCI versus medical therapy in stable coronary disease. N Engl J Med. 2012; 367: 991–1001. doi: 10.1056/NEJMoa1205361 PMID: 22924638
9. Pijls NHJ, Sels JEM. Functional measurement of coronary stenosis. JACC. Elsevier Inc.; 2012; 59: 1045–1057. doi: 10.1016/j.jacc.2011.09.077
10. Tonino PAL, De Bruyne B, Pijls NHJ, Siebert U, Ikeno F, van't Veer M, et al. Fractional flow reserve versus angiography for guideing percutaneous coronary intervention. N Engl J Med. 2009; 360: 213–224. doi: 10.1056/NEJMoa0807611 PMID: 19144937
11. Johnson NPP, Kirkeeide RLL, Gould KLL. Is discordance of coronary flow reserve and fractional flow reserve due to methodology or clinically relevant coronary pathophysiology? JACC Cardiovasc Imaging. 2012; 5: 193–202. doi: 10.1016/j.jcmg.2011.09.020 PMID: 22340827
12. Sen S, Escaned J, Malik IS, Mikhail GW, Foale RA, Mila R, et al. Development and validation of a new adenosine-independent index of stenosis severity from coronary waveintensity analysis: Results of the ADVISE (ADenosine Vasodilator Independent Stenosis Evaluation) study. J Am Coll Cardiol. 2012; 59: 1392–1402. doi: 10.1016/j.jacc.2011.11.003 PMID: 22154731
13. Tu S, Barbato E, Köszegi Z, Yang J, Sun Z, Holm NR, et al. Fractional flow reserve calculation from 3-dimensional quantitative coronary angiography and TIMI frame count: A fast computer model to quantify the functional significance of moderately obstructed coronary arteries. JACC Cardiovasc Interv. 2014; 7: 768–777. doi: 10.1016/j.jcin.2014.03.004 PMID: 25060020
14. Kim H, Vignon-Clementel I, Coogan J, Figueroa C, Jansen K, Taylor C. Patient-specific modeling of blood flow and pressure in human coronary arteries. Ann Biomed Eng. 2010; 38: 3195–3209. doi: 10.1007/s10439-010-0083-6 PMID: 20559732

15. Kim HJ, Vignon-Clementel IE, Figueroa CA, Ladisa JF, Jansen KE, Feinstein JA TC. On coupling a lumped parameter heart model and a three-dimensional finite element aorta model. Ann Biomed Eng. 2009; 37: 2153–2169. doi: 10.1007/s10439-009-9760-8 PMID: 19609676

16. Koo B-K, Erglis A, Doh J-H, Daniels D V, Jegere S, Kim H-S, et al. Diagnosis of ischemia-causing coronary stenoses by noninvasive fractional flow reserve computed from coronary computed tomographic angiograms. Results from the prospective multicenter DISCOVER-FLOW (Diagnosis of Ischemia-Causing Stenoses Obtained via Noni. J Am Coll Cardiol. 2011; 58: 1989–1997. doi: 10.1016/j.jacc.2011.06.066 PMID: 22032711

17. Min JK, Koo B, Erglis A, Doh J, Daniels D V, Jegere S, et al. Usefulness of noninvasive fractional flow reserve computed from coronary computed tomographic angiograms for intermediate stenoses confirmed by quantitative coronary angiography. AJC. 2012; 110: 971–976. doi: 10.1016/j.amjcard.2012.05.033

18. Min JK, Min JK, Leipsic J, Pencina MJ, Berman DS, Koo BK, van Mieghem C, Erglis A, Lin FY, Dunning AM, Apruzzese P, Budoff MJ, Cole JH, Jaffer FA, Leon MB, Malpeso J, Mancini GB, Park SJ, Schwartz RS, Shaw LJ ML. Diagnostic accuracy of fractional flow reserve from anatomic CT angiography. JAMA. 2012; 308(12):1237–1245. doi: 10.1001/2012.jama.11274 PMID: 22922562

19. Nørgaard B, Leipsic J, Gaur S, Seneviratne S, Ko BS, Ito H, et al. Diagnostic performance of non-invasive fractional flow reserve derived from coronary CT angiography in suspected coronary artery disease: The NXT trial. J Am Coll Cardiol. 2014; 63: 1145–1155. doi: 10.1016/j.jacc.2013.11.043 PMID: 24486266

20. Taylor CA, Fonte TA, Min JK, City R, Angeles L. Computational fluid dynamics applied to cardiac computed tomography for noninvasive quantification of fractional flow reserve: scientific basis. J Am Coll Cardiol. 2013; 61: 2233–2241. doi: 10.1016/j.jacc.2012.11.083 PMID: 23562923

21. Coenen A, Lubbers M, Kurata A, Kono A, Dedic A, Chelu R, et al. Fractional flow reserve computed from noninvasive CT angiography data: diagnostic performance of an on-site clinician-operated computational fluid dynamics algorithm. Radiology. 2015; 274(3): 674–683. doi: 10.1148/radiol.14140992 PMID: 25322342

22. Zhang J, Luo T, Tan S, Lomarda A, Wong A, Keng F, et al. Hemodynamic analysis of patient-specific coronary artery tree. Int J Numer Methods Biomed Eng. 2015; 31: e02708. doi: 10.1002/cnm .2708

23. Huo Y, Svendsen M, Choy JS, Zhang Z-D, Kassab GS. A validated predictive model of coronary fractional flow reserve. Journal of The Royal Society Interface. 2012; 9(71): 1325–1338. doi: 10.1098/rsif.2011.0605

24. Abbara S, Arbab-Zadeh A, Callister TQ, Desai MY, Mamuya W, Thomson L, et al. SCCT guidelines for performance of coronary computed tomographic angiography: A report of the Society of Cardiovascular Computed Tomography Guidelines Committee. J Cardiovasc Comput Tomogr. 2009; 3: 190–204. doi: 10.1016/j.jcct.2009.03.004 PMID: 19409872

25. Bashore TM, Balter S, Barac A, Byrne JG, Cavendish JJ, Chambers CE, et al. 2012 American college of cardiology foundation/society for cardiovascular angiography and interventions expert consensus document on cardiac catheterization laboratory standards update. Journal of the American College of Cardiology. 2012; 59 (24): 2221–2305. doi: 10.1016/j.jacc.2012.02.010 PMID: 22575325

26. Schlundt C, Bietau C, Klinghammer L, Wiedemann R, Rittger H, Ludwig J, et al. Comparison of intracoronary versus intravenous administration of adenosine for measurement of coronary fractional flow reserve. Circ Cardiovasc Interv. 2015; 8: e001781. doi: 10.1161/CIRCINTERVENTIONS.114.001781 PMID: 25908694

27. Koller TM, Gerig G, Szekely G, Dettwiler D. Multiscale detection of curvilinear structures in 2-D and 3-D image data. Proc IEEE Int Conf Comput Vis. 1995; 1995: 864–869. doi: 10.1109/ICCV.1995.466846

28. Boykov Y, Veksler O, Zabih R. Fast approximate energy minimization via graph cuts. Pattern Anal Mach Intell IEEE Trans. 2001; 23: 1222–1239. doi: 10.1109/34.969114

29. Luo T, Wischgoll T, Koo BK, Huo Y, Kassab GS. IVUS validation of patient coronary artery lumen area obtained from CT images. PLoS One. 2014; 9: 1–7. doi: 10.1371/journal.pone.0086949

30. Arbab-Zadeh A, Hoe J. Quantification of coronary arterial stenoses by multidetector CT angiography in comparison with conventional angiography: Methods, caveats, and implications. JACC Cardiovasc Imaging. Elsevier Inc.; 2011; 4: 191–202. doi: 10.1016/j.jcmg.2010.10.011

31. Yamano T, Tanaka A, Tanimoto T, Takarada S, Kitabata H, Kuroi A, Imanishi T AT. Optimal threshold for multi detector computer tomography to detect physiologically significant stenosis in patients with ischemic heart disease. Circulation. 2008; 118: S_106.

32. Hamada M, Kuwahara T, Shigematsu Y, Kodama K, Hara Y, Hashida H, et al. Relation between coronary blood flow and left ventricular mass in hypertension: noninvasive quantification of coronary blood flow by thallium-201 myocardial scintigraphy. Hypertens Res. 1998; 21: 227–234. PMID: 9877515

33. Wieneke H, von Birgelen C, Haude M, Eggebrecht H, Möhlenkamp S, Schmermund A, et al. Determinants of coronary blood flow in humans: quantification by intracoronary Doppler and ultrasound. Journal of Applied Physiology 2005; 98(3):1076–1082. doi: 10.1152/japplphysiol.00724.2004

34. Zhou Y, Kassab GS, Molloi S. On the design of the coronary arterial tree: a generalization of Murray's law. Phys Med Biol. 1999; 44: 2929–2945. doi: 10.1088/0031-9155/44/12/306 PMID: 10616146

35. Wilson RF, Wyche K, Christensen BV, Zimmer S LD. Effects of adenosine on human coronary arterial circulation. Circulation. 1990; 82: 1595–1606. doi: 10.1161/01.CIR.82.5.1595 PMID: 2225364

36. Sianos G, Morel M-A, Kappetein AP, Morice M- C, Colombo A, Dawkins K, et al. The SYNTAX Score: an angiographic tool grading the complexity of coronary artery disease. EuroIntervention. 2005; 1: 219–227. EIJV1I2A36 [pii] PMID: 19758907

37. Meijboom WB, Van Mieghem CAG, van Pelt N, Weustink A, Pugliese F, Mollet NR, et al. Comprehensive assessment of coronary artery stenoses. Computed tomography coronary angiography versus conventional coronary angiography and correlation with fractional flow reserve in patients with stable angina. J Am Coll Cardiol. 2008; 52: 636–643. doi: 10.1016/j.jacc.2008.05.024 PMID: 18702967

38. Gould KL, Johnson NP. Coronary artery disease: percent stenosis in CAD-a flaw in current practice. Nat Rev Cardiol. 2010; 7(9): 482–484. doi: 10.1038/nrcardio.2010.119 PMID: 20725105

39. White CW, Wright CB, Doty DB, Hiratza LF, Eastham CL, Harrison DG, et al. Does visual interpretation of the coronary arteriogram predict the physiologic importance of a coronary stenosis? N Engl J Med. 1984; 310: 819–824. doi: 10.1056/NEJM198403293101304 PMID: 6700670

40. Zhang JM, Zhong L, Su B, Wan M, Yap JS, Tham JPL, et al. Perspective on CFD studies of coronary artery disease lesions and hemodynamics: A review. Int J Numer Methods Biomed Eng. 2014; 30: 659–680. doi: 10.1002/cnm.2625

41. Thompson AG, Raju R, Blanke P, Yang T, Mancini GBJ, Budoff MJ, et al. Diagnostic accuracy and discrimination of ischemia by fractional flow reserve CT using a clinical use rule: Results from the Determination of Fractional Flow Reserve by Anatomic Computed Tomographic Angiography study. J Cardiovasc Comput Tomogr. Elsevier Inc; 2015; 9: 120–128. doi: 10.1016/j.jcct.2015.01.008 PMID: 25819194

42. Molloi S, Ersahin A, Tang J, Hicks J, Leung CY. Quantification of volumetric coronary blood flow with dual-energy digital subtraction angiography. Circulation. 1996; 93: 1919–1927. doi: 10.1161/01.CIR.93.10.1919 PMID: 8635272

43. Molloi S, Zhou Y, Kassab GS. Regional volumetric coronary blood flow measurement by digital angiography: In vivo validation. Acad Radiol. 2004; 11: 757–766. doi: 10.1016/j.acra.2004.04.002 PMID: 15217593

44. Min JK, Taylor CA, Achenbach S, Koo BK, Leipsic J, Nørgaard BL, et al. Noninvasive Fractional Flow Reserve Derived From Coronary CT Angiography. JACC Cardiovasc Imaging. 2015; 8: 1209–1222. doi: 10.1016/j.jcmg.2015.08.006 PMID: 26481846

45. Qiu Y, Tarbell JM. Numerical simulation of pulsatile flow in a compliant curved tube model of a coronary artery. J Biomech Eng. 2000; 122: 77–85. doi: 10.1115/1.429629 PMID: 10790833

46. Ramaswamy SD, Vigmostad SC, Wahle A, Lai YG, Olszewski ME, Braddy KC, et al. Fluid dynamic analysis in a human left anterior descending coronary artery with arterial motion. Ann Biomed Eng. 2004; 32: 1628–1641. doi: 10.1007/s10439-004-7816-3 PMID: 15675676

47. Petraco R, Escaned J, Sen S, Nijjer S, Asrress KN, Echavarria-Pinto M, et al. Classification performance of instantaneous wave-free ratio (iFR) and fractional flow reserve in a clinical population of intermediate coronary stenoses: Results of the ADVISE registry. EuroIntervention. 2013; 9: 91–101. doi: 10.4244/EIJV9I1A14 PMID: 22917666